HNUE JOURNAL OF SCIENCE DOI: 10.18173/2354-1059.2023-0028
Natural Sciences 2023, Volume 68, Issue 2, pp. 138-149
This paper is available online at http://stdb.hnue.edu.vn

FACILE SYNTHESIS OF Ni-Co-S ON Ni FOAM AS ELECTROCATALYST FOR OXYGEN EVOLUTION REACTION

Luong Thi Thu Thuy and Le Van Khu*
Faculty of Chemistry, Hanoi National University of Education

Abstract. Ni-Co-S electrocatalysts for oxygen evolution reaction (OER) are fabricated on nickel foam using a one-step hydrothermal method. The as-prepared materials were characterized using a scanning electron microscope (SEM), energy-dispersive X-ray spectroscopy (EDX), X-ray diffraction analysis (XRD), and cyclic voltammetry (CV). With the presence of Co, both the double-layer capacitance and the surface concentration of the redox active site increase, resulting in an improvement in OER catalytic activity in the basic medium. The sample prepared with the 1/1 ratio of Ni/Co shows the best electrocatalytic performance with the low overpotential of 276 mV at a current density of 10 mA cm^{-2} and a Tafel slope of 51.3 mV dec^{-1} and exhibits good stability in the OER.

Keywords: nickel sulfide, cobalt sulfide, hydrothermal method, oxygen evolution reaction.

1. Introduction

Hydrogen is regarded as an attractive material for alternative energy to replace fossil fuels thanks to its environmental friendliness and high calorific value. Hydrogen production via electrolysis has the advantages of high efficiency, excellent adaptability, and nearly zero carbon emissions [1]. Nevertheless, one of the critical barriers that limit its application is the high overpotential of the formation of gasses [2], especially the evolution of O_2, which involves the transfer of four electrons. To date, Ru/Ir-based compounds are proven to be efficient electrocatalysts for the oxygen evolution reaction (OER), but it is unstable in alkaline media and is restricted by their high price and scarcity [3]. Therefore, it is highly desirable to develop cost-effective, abundant, and efficient electrocatalysts for OER.

Concerning the above matter, non-noble transition metal sulfides, particularly bifunctional electrocatalysts, have received great attention due to their distinctive structural features, rich active sites, and adjustable electronic properties and components [4]. With various valences, nickel could undergo different electronic transitions and is a good candidate for electrocatalysts [5]. Previous research unraveled that the presence of

Received June 5, 2023. Revised June 16, 2023. Accepted June 23, 2023.
Contact Le Van Khu, e-mail address: khulv@hnue.edu.vn

Co can immensely boost the electrocatalytic activity of the catalyst by changing electron distribution and optimizing the adsorption energy of NiS. Wang et al. used two-step electrodeposition to prepare Co-NiS-NF that can lower the overpotential to less than 300 mV at a current density of 20 mA cm^{-2} [6]. Bu et al. employed solvothermal processes to first synthesize MOF precursor and then Co_9S_8-Ni_3S_2/NF to achieve an overpotential of 233 mV at a current density of 10 mA cm^{-2} and corresponding Tafel slope of 116.75 mV dec^{-1} [7]. Tong et al. reported an atomic layer deposition to form CoO film and later synthesis of the Co12@Ni_3S_2/NF by hydrothermal at 150°C for 5h in a vacuum oven. The product showed excellent catalytic activity with a small overpotential of 297 mV at 20 mA cm^{-2} and a Tafel slope of 50.3 mV dec^{-1} [8]. The performance of these catalysts is relatively good, but the synthesis process is difficult to achieve.

Herein, Ni-S and Co-Ni-S samples were fabricated on nickel foam via a simple method of one-step hydrothermal and thereafter were used as electrodes for the OER in alkaline electrolyte. The electrochemical properties and electrocatalytic performance of the as-prepared electrodes were investigated.

2. Content

2.1. Experimental procedure

2.1.1. Materials preparation

The materials and chemicals used in this study all originated from China. Nickel foam (NF) with a thickness of 0.5 mm was cut into rectangular pieces with dimensions of 10 mm × 50 mm, soaked in ~1.0 M HCl solution for 30 min, and then washed several times with distilled water (in combination with ultrasound) and with acetone. The NF was then air-dried at 80°C and limited to ~1 cm^2 working area by a Teflon tape. 0.1 M $Ni(NO_3)_2$, 0.1 M $Co(NO_3)_2$, 0.3 M $(NH_2)_2CS$ stock solutions, and 1.0 M KOH electrolyte were prepared from the solids $Ni(NO_3)_2.6H_2O$, $Co(NO_3)_2.6H_2O$, $(NH_2)_2CS$ and KOH, respectively.

NiCo-S materials were synthesized on NF by hydrothermal methods as follows: NF was soaked in a 50 mL mixed solution of $Ni(NO_3)_2$ and $Co(NO_3)_2$ with a total concentration of 0.02 M ($Ni(NO_3)_2$/ $Co(NO_3)_2$ ratio of 3/1, 1/1, 1/3, and 1/0, respectively) and 0.06 M $(NH_2)_2CS$. These solutions were made from the stock solutions above. Thereafter, the system was placed in a Teflon bottle in the autoclave at 140°C for 6 h. After being naturally cooled to room temperature, the samples were removed from the reaction vessel, washed several times with distilled water, rinsed with acetone, and dried in air at 80°C for 15 h. The obtained samples were labelled as 3Ni1Co-S, 1Ni1Co-S, 1Ni3Co-S, and Ni-S, corresponding to the $Ni(NO_3)_2$/$Co(NO_3)_2$ ratio used.

2.1.2. Characterization

SEM images of the samples were taken on a Hitachi-S4800 scanning electron microscope. EDX spectra were characterized on a Horiba 7593H energy dispersive X-ray analyzer. XRD patterns were recorded on a Brucker-D8 Advance diffractometer.

The electrochemical characteristics of the samples were determined on a VMP3 Multichannel Potentiostat with a three-electrode cell. The reference electrode, counter electrode, and working electrode are saturated calomel electrode (SCE), Pt foil (~2 cm^2), and the as-prepared electrodes, respectively. Measurements were performed in 1.0 M KOH solution at room temperature (25°C). Before testing, dissolved O_2 was removed by N_2 bubbling for 30 min. The measured potentials are *iR*-corrected for the solution resistances according to the following equation:

$$E_{iR\text{-corrected}} = E_{measured} - iR \quad (1)$$

where *i* is the current and *R* is the ohmic electrolyte resistance measured by electrochemical impedance spectroscopy.

For ease of comparison, all potentials reported in this manuscript were converted to the reversible hydrogen electrode (RHE) according to the following equation:

$$E_{RHE} = E_{SCE} + \frac{2.303RT}{F}pH + E^{o}_{SCE} \quad (2)$$

At 25°C, the measured pH value of 1.0 M KOH is 13.65 [9] and $E^{o}_{SCE} = 0.2412\,V$ *vs.* RHE, so $E_{RHE} = E_{SCE} + 0.05916 \times 13.65 + 0.2412 = E_{SCE} + 1.0487$, where $E_{SCE} = E_{iR\text{-corrected}}$.

2.2. Results and discussion

2.2.1. Physical properties

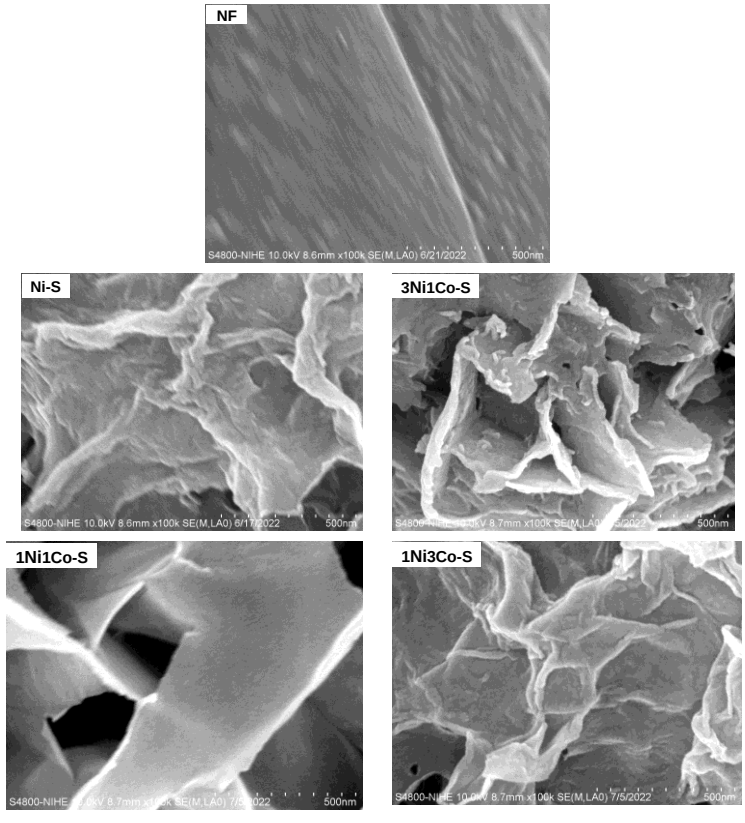

Figure 1. SEM images of the as-prepared samples

Figure 1 presents SEM images of the synthesized samples. For comparison, Figure 1 also introduces SEM images of NF. It can be seen that the surface of the NF is relatively flat and even. All the as-prepared materials consist of nanoflake arrays which are aggregated loosely to create porosity for the material. On the surface of the 3Ni1Co-S sample, there are also small particles that increase the roughness of the material. The large specific surface area and porous structure ensure good contact between the catalyst and an electrolyte and take full advantage of the synthesized material.

A typical EDX spectrum of the 1Ni1Co-S sample in Figure 2 shows that Ni, Co, and S were mostly present. There is no characteristic peak of N, which proves that the NO_3^- ion has been removed from the material during the washing procedure after synthesis. Three spots on each sample were used for the EDX analysis, and the average percentage of the elements was shown in Table 1. It can be seen that Ni makes up the largest percentage, which might come from the synthesized NiS and nickel foam substrate. Nevertheless, the percentage of Ni and Co are in accordance with the ratio of the starting materials.

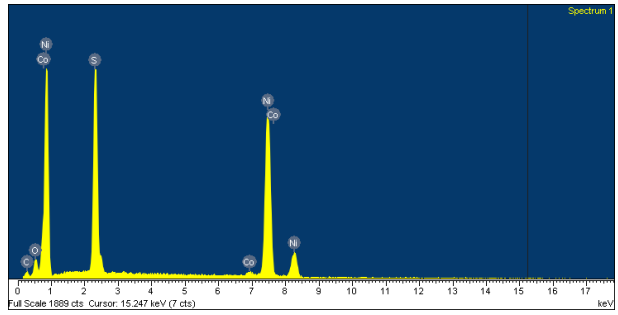

Figure 2. EDX spectrum of 1Ni1Co-S sample

Table 1. Elemental composition of the as-prepared samples

Sample	Weight percentage (%)					
	C	**O**	**S**	**Co**	**Ni**	**Total**
Ni-S	1.25	2.00	26.55	0	70.20	100
3Ni1Co-S	2.86	3.00	24.29	2.26	67.60	100
1Ni1Co-S	2.37	5.62	20.88	4.34	66.79	100
1Ni3Co-S	3.20	7.89	16.00	6.95	65.96	100

The results obtained from the X-ray diffraction test (not shown here) indicate that the synthesized sample on NF is in amorphous form since the XRD pattern exhibits only two diffraction peaks at $2\theta = 44.5^o$ and 50.8^o which corresponds to the planes of reflection of (111) and (200) of nickel [10].

2.2.2. Electrochemical characterization

In Figure 3, the cyclic voltammetry (CV) curves of the as-prepared materials are recorded at a 2 mV/s scan rate within a potential window of 0.8~1.6 V *vs* RHE in 1.0 M KOH electrolyte. For comparison, this figure also shows the CV curve of NF. It can be

seen that the CV curves of the samples can be divided into three parts corresponding to three reduction potential ranges.

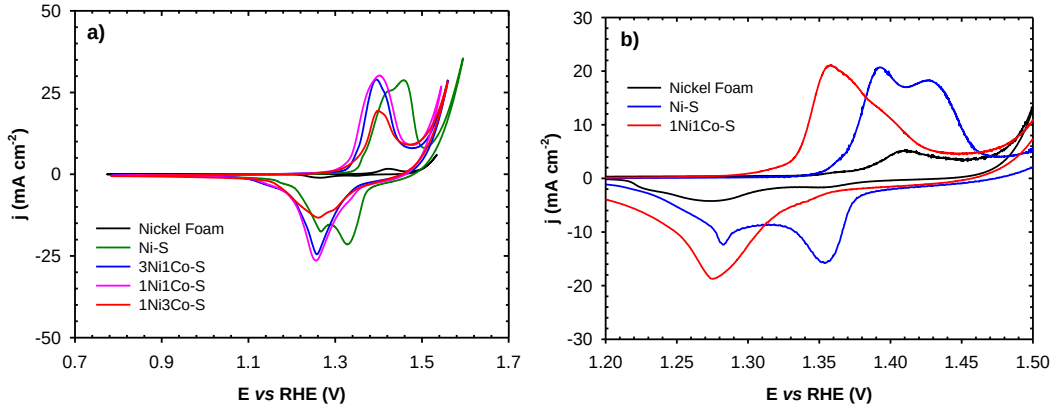

Figure 3. CV curves in 1.0 M KOH electrolyte: a) of NF and the as-prepared samples at a scan rate of 2 mV s^{-1} and b) of NF, Ni-S and 1Ni1Co-S at a scan rate of 1 mV s^{-1} (The current density of the NF sample is amplified by 10 times)

In the range of E = 0.8 – 1.1V vs. RHE, there is no reduction peak, but the current density is different from 0. This phenomenon is explained by the effect of the electric double layer on the electrode surface.

In the range of E > 1.55 V vs RHE, the OER happens according to the electrode reaction.

$$4OH^- \rightarrow O_2 + 2H_2O + 4e^- \quad (3)$$

In the range of E = 1.1 – 1.55 V vs. RHE, there are oxidation and reduction peaks that are assigned to the oxidation and reduction processes of Ni and Co compounds on the electrode surface, two redox peaks for Ni-S sample, and only one redox peak for Ni-Co-S sample. To clarify the occurrence of these peaks, CV curves at a scan rate of 1 mV s^{-1} were recorded for NF, Ni-S, and 1Ni1Co-S samples (the current density of the NF sample is amplified by 10 times to facilitate observation) (Figure 3b). There is one reduction peak at ~1.28 V *vs.* RHE and one oxidation peak at ~1.4V *vs.* RHE for the NF sample, which could be assigned to the reduction of Ni(III) to Ni(II) and the oxidation of Ni(II) to Ni(III) according to the equation (4) [11].

$$Ni(OH)_2 + OH^- \rightleftharpoons NiOOH + H_2O + e^- \quad (4)$$

In an alkaline solution, Ni can form different hydroxides, α-$Ni(OH)_2$ and β-$NiOH)_2$. And when oxidized it will form γ-NiOOH and β-NiOOH, respectively. Therefore, the presence of two redox peaks can be ascribed to two oxidation reactions α-$Ni(OH)_2$ → γ-NiOOH, β-$NiOH)_2$ → β-NiOOH and the latter occurring at a higher anodic potential [5]. For samples containing Co, the appearance of only one pair of oxidation-reduction peaks can be explained by the interaction between Ni, Co, and O to produce a more stable compound. As shown in the EDX analysis, the presence of increasing Co concentrations gradually increased the amount of O and gradually decreased the amount of S in the material samples. This also causes the reduction and oxidation peaks to shift slightly to a smaller potential region than in the absence of Co.

In order to determine the electrochemical properties of the as-prepared samples in more detail, the CV data were exploited at different potential intervals.

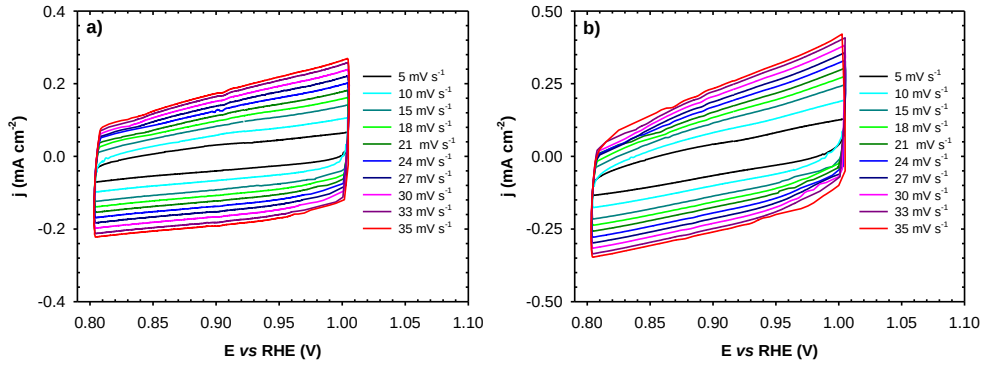

Figure 4. CV curves of a) Ni-S, and b) 1Ni1Co-S in the non-Faradic region at different scan rates

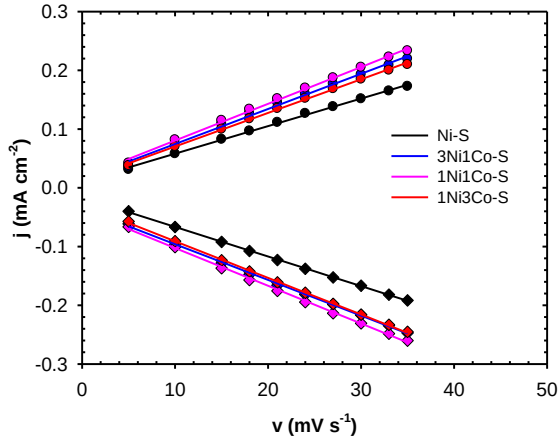

Figure 5. Anodic and cathodic charging current densities measured at 0.9 V vs. RHE plotted as a function of scan rate

(i) In the non-Faradic region from 0.8 to 1.0 V vs RHE, the CV at scan rate from 5 to 35 mV/s was recorded for Ni-S and 1Ni1Co-S samples and illustrated in Figure 4. The near parallelogram shape of the CV curves is typical for the capacitive properties of the electrical double layer on the surface of the electrode material. There exists a little deformation in the corner of the rectangular shape, which is caused by the resistance of the solution and the measuring system. The unchanged shape of the CV curves up to 35 mV s^{-1} demonstrates rapid ion transportation and a good scan rate capability. To calculate the average double layer capacitance (C_{dl}) at E = 0.9 V vs. RHE, the cathodic and anodic current densities at this potential were plotted as a function of scan rate and shown in Figure 5. From the slopes of these lines, C_{dl} was calculated according to equation (5) [12] and summarized in Table 2.

$$i = C_{dl}\frac{dE}{dt} = C_{dl}v \qquad (5)$$

It can be seen that the double-layer capacitance of the sample is between 4.86 and 6.35 mF cm^{-2}. The introduction of Co to the Ni-S material increases the double layer capacitance from 4.86 to higher than 5.98 mF cm^{-2}, in particular, the 1Ni1Co-S shows the highest C_{dl} of 6.35 mF cm^{-2}. This improvement in capacitance might be due to the

more ion-accessible sites resulting from the large exposed active surface area [13] that in turn could exhibit better electrocatalytic activity.

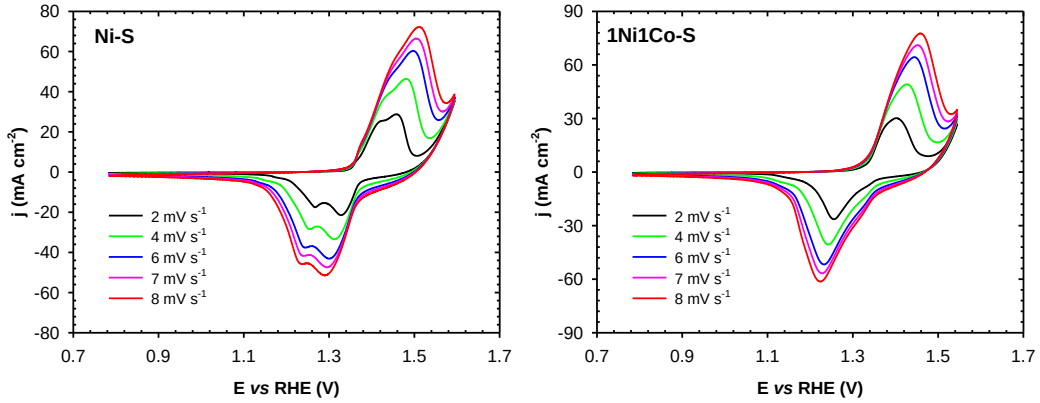

Figure 6. CV curves of Ni-S and 1Ni1Co-S in 1M KOH electrolyte at different scan rates

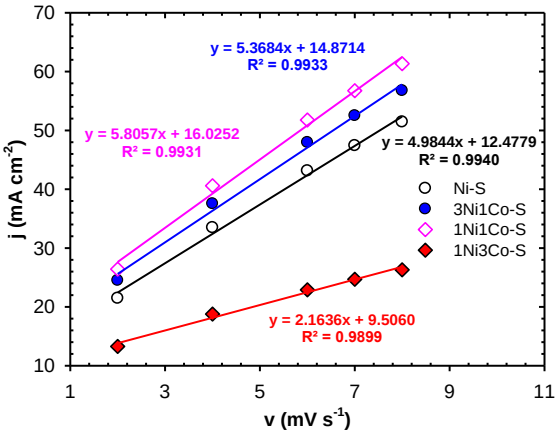

Figure 7. Cathodic peak densities as a function of scan rate

(ii) In the Faradic region of 1.1~1.6 V, CV measurements were conducted at different scan rates (2 to 8 mV s^{-1}) to determine the surface concentration of the redox active site (Γ_o). Typical CV curves of Ni-S and 1Ni1Co-S samples were illustrated in Figure 6. The Γ_o was deduced from the slope of the linear relationship between the current of the reduction peak and the scan rate, following the equation (6) [14]:

$$\text{slope} = \frac{n^2F^2A\Gamma_o}{4RT} \quad (6)$$

where n = 1, F = Faraday's constant, A = surface area, Γ_o = surface concentration of redox active site, R = ideal gas constant, and T = temperature.

The reduction peak current is plotted against the scan rates and the calculated value of the surface concentration of the redox active site was summarized in Table 2. Γo was only 5.32 μmol cm^{-2} in the Ni-S sample but increase to 5.73 μmol cm^{-2} in the 3Ni1Co-S sample and 6.20 μmol cm^{-2} in the 1Ni1Co-S sample. This might be explained by the

synergistic effect of Co [15]. However, the Co/Ni ratio in the starting sample increased to 3/1 (1Ni3Co-S), Γo on the contrary decreased to 2.31 μmol cm^{-2}.

Table 2. Double layer capacitances of the samples at E = 0.90 V vs. RHE and the surface concentration of the redox-active site

Sample	Double layer capacitance (C_{dl}, mF cm^{-2})	The surface concentration of the redox-active site (Γ_o, μmol cm^{-2})
Ni-S	4.86	5.32
3Ni1Co-S	6.03	5.73
1Ni1Co-S	6.35	6.20
1Ni3Co-S	5.98	2.31

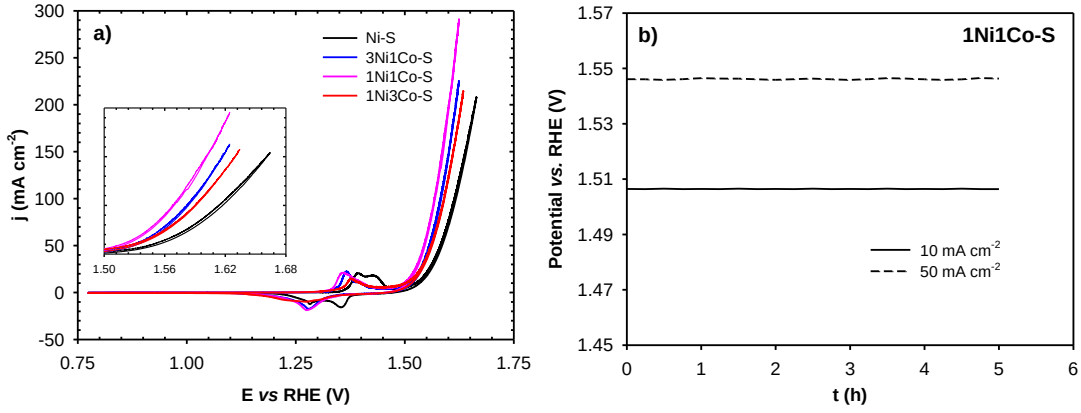

Figure 8. a) CV curves at a scan rate of 1 mV s^{-1} and b) chronopotentiometry curves at difference current density of 1Ni1Co-S of 1Ni1Co-S

(iii) To exploit the OER potential region, the CV curves with a scan rate of 1 mV s^{-1} of the prepared samples were recorded and presented in Figure 8a. A hysteresis loop can be observed in the 1.5~1.6 region (the inserted picture) which is probably due to the hindering effect of the bubbling of O_2 escape on the electrode surface. Of all the electrodes investigated, in the potential of OER region the current density of 1Ni1Co-S is higher than that of other electrodes, showing the best catalytic activity among the studied samples. To determine the electrocatalytic activity for the OER of the samples, the overpotential (η) at a current density (j) of 10 mA cm^{-2} was calculated using the following equation:

$$\eta = E_{RHE} - 1.229 \quad (7)$$

The obtained overpotential of this study and some other similar studies are summarized in Table 3. The overpotential at 10 mA cm^{-2} of the prepared electrodes is within 276-304 mV and follows the order: 1Ni1Co-S < 1Ni3Co-S < 3Ni1Co-S < Ni-S. The 1Ni1Co-S sample displayed the lowest overpotential of 276 mV at 10 mA cm^{-2}. This proves that the 1Ni1Co-S sample has the best electrocatalytic performance for the

OER process and can be explained by the fact that this sample exhibit the largest exposed active surface area and the highest value of the surface concentration of the redox-active site as discussed above.

It is also found from Table 3 that the overpotential at 10 mA cm^{-2} of the 1Ni1Co-S sample is approximately the same as that of similar materials. In addition, the experiment results show that this electrode can function well at high current density. It reaches current densities of 50 and 100 mA cm^{-2} at an overpotential of 317 and 340 mV respectively, and in particular, this sample achieved a current density as high as 260 mA cm^{-2} at an overpotential of 387 mV.

Table 3. Overpotential at 10 mA cm^{-2} current densities of some catalysts for OER

Sample	Substrate	η (mV) @ 10 mA cm^{-2}	Ref.
Ni-S	NF	304	This study
3Ni1Co-S	NF	287	This study
1Ni1Co-S	NF	276	This study
1Ni3Co-S	NF	285	This study
$Ni_{0.3}Fe_{0.07}Co_{0.2}Ce_{0.43}O_x$	GC	370	[16]
Co-Ni_3S_2	NF	274	[17]
$Ni_{0.25}CO_{0.75}(OH)_2$	GC	352	[18]
NiCo-LDHs	NF	367	[19]

The catalytic stability of the typical sample 1Ni1Co-S was studied at current densities of 10 mA cm^{-2} and 50 mA cm^{-2} and the results were shown in Figure 8b. It can be seen that the 1Ni1Co-S sample exhibits good stability after 5 hours of continuous testing without any increase in potential. These results make it a promising anode electrocatalyst for practical applications of water splitting.

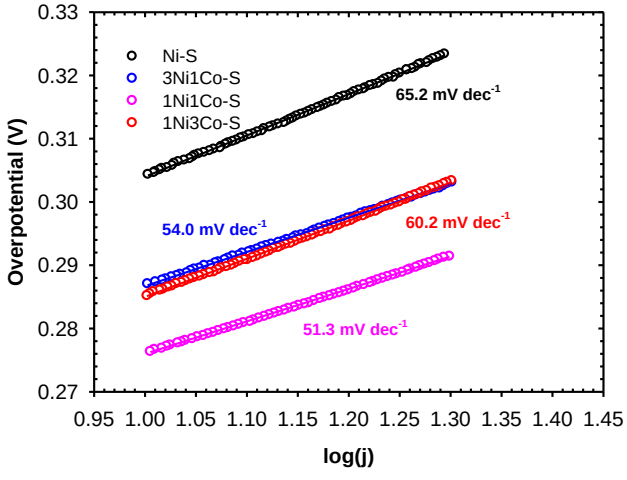

Figure 9. Tafel plots of the as-prepared samples in 1 M KOH electrolyte

Tafel slopes are used to determine the kinetics of the OER process. A low Tafel slope results in a fast increase in the current density through a small increase in overpotential indicating fast electrochemical kinetics of the OER. Besides, a Tafel slope may provide insightful information about the reaction mechanism of the target system. Tafel slopes were calculated by fitting polarization data to the Tafel equation (8) and illustrated in Figure 9.

$$\eta = a + b*\log|j| \quad (8)$$

where *a* is a constant and b is the Tafel slope.

The OER is known as a 2 or 4 electron step, and the reaction mechanism is complicated. Based on the literature, we considered the mechanism under alkaline conditions following the Krasil'shchikov path [20]

$$M + OH^- \rightarrow MOH + e^- \quad (9)$$

$$MOH + OH^- \rightarrow MO^- + H_2O \quad (10)$$

$$MO^- \rightarrow MO + e^- \quad (11)$$

$$2MO \rightarrow O_2 + 2M \quad (12)$$

where M stands for an empty active site. Typically, OH^- first adsorbs on the empty active site to form the adsorbed MOH (Equation 9). This adsorbed MOH intermediate adsorbs another OH^- to form adsorbed MO^- (Equation 10). The adsorbed MO^- intermediate gives up an electron to form adsorbed MO (Equation 11). Finally, the two MO intermediates react with each other to form O_2 and free the active site (Equation 12).

According to the literature, the Tafel slope of 60 mV dec^{-1} and 40 mV dec^{-1} suggests that steps (10) and (11) respectively determine the overall rate [20]. The Tafel slope of the prepared samples is in the range of 51.3 – 65.2 mV dec^{-1}. These Tafel slopes are near 60 mV dec^{-1}, indicating that the OER on the prepared samples may be controlled by the formation of MO^- intermediate. The lowest Tafel slope of 51.3 mV s^{-1} (near 40 mV dec^{-1}) indicating the OER process may be controlled also by the formation of the MO intermediate [20].

3. Conclusions

In this study, Ni-S and Ni, Co-S materials were successively synthesized on nickel foam by hydrothermal method. The samples are in an amorphous form consisting of small pieces arranged loosely to create porosity. Ni, Co-S materials exhibit better electrocatalytic activity for the OER process than Ni-S materials due to the synergetic effect of Co. The catalytic performance depends on the ratio of Ni/Co in the synthesized solution. The sample prepared with Ni/Co equal 1/1 (1Ni1Co-S) exhibits superior catalytic activity for OER in basic medium with low overpotentials of 276 mV and 387 mV at a current density of 10 mA cm^{-2} and 260 mA cm^{-2}, respectively. In this sample, the formation of MOH and MO may be the controlled steps in the mechanism of the OER process.

REFERENCES

[1] Li X, Zhou Y, Feng C, Wei R, Hao X, et al., 2022. High entropy materials based electrocatalysts for water splitting: Synthesis strategies, catalytic mechanisms, and prospects. *Nano Research*, Vol. 16, pp. 4411-4437.

[2] Luo J, Im J-H, Mayer MT, Schreier M, Nazeerunddin MK, et al., 2014. Water photolysis at 12.3% efficiency via perovskite photovoltaics and Earth-abundant catalysts. *Science*, Vol. 345, pp. 1593.

[3] Rao RR, Kolb MJ, Giordano L, Perdersen AF, Katayama Y, et al., 2020. Operando identification of site-dependent water oxidation activity on ruthenium dioxide single-crystal surfaces. *Nat. Catal*., Vol. 3, pp. 516–525.

[4] Wang M, Zhang L, He Y, Zhu H, 2021. Recent advances in transition-metal-sulfide-based bifunctional electrocatalysts for overall water splitting. *Journal of Material Chemistry A*, Vol. 9, pp. 5320-5363.

[5] Angeles-Olvera Z, Crespo-Yapur A, Rodríguez O, Cholula-Díaz JL, Martínez LM, et al., 2022. Nickel-Based Electrocatalysts for Water Electrolysis. *Energies*, Vol. 15, pp. 1609.

[6] Wang X, Li L, Xu L, Wang Z, Wu Z, et al., 2021. An efficient and stable MnCo@NiS catalyst for oxygen evolution reaction constructed by a step-by-step electrodeposition way. *Journal of Power Sources*, Vol. 489, pp. 229525.

[7] Bu Y, Zhang Y, Liu Y, Li S, Zhou Y, et al., 2023. MOF-derived urchin-like Co_9S_8-Ni_3S_2 composites on Ni foam as efficient self-supported electrocatalysts for oxygen evolution reaction. *Batteries*, Vol. 9, pp. 46.

[8] Tong X, Li Y, Pang N, Qu Y, Yan C, et al., 2021. Co-doped Ni_3S_2 porous nanocones as high-performance bifunctional electrocatalysts in water splitting. *Chemical Engineering Journal*, Vol. 425, pp. 130455.

[9] Niu S, Li S, Du Y, Han X, Xu P, 2020. How to reliably report the overpotential of an electrocatalyst. *ACS Energy Letters*, Vol. 5, pp. 1083-1087.

[10] Cheng G, Bai Q, Si C, Yang W, Dong C, et al., 2015. Nickel oxide nanopetal-decorated 3D nickel network with enhanced pseudocapacitive properties. *RSC Advances*. Vol. 5, Iss. 20, pp. 15042-15051.

[11] Salleh NA, Kheawhom S, Mohamad AA, 2020. Characterizations of nickel mesh and nickel foam current collectors for supercapacitor application. *Arabian Journal of Chemistry*, Vol. 13, pp. 6838.

[12] Connor P, Schuch, Kaiser J, Kaiser B, Jaegermann W, 2020. The Determination of Electrochemical Active Surface Area and Specific Capacity Revisited for the System MnO_x as an Oxygen Evolution Catalyst. *Zeitschrift für Physikalische Chemie*, Vol. 234, pp. 979-994.

[13] Li M, Xu Z, Li Y, Wang J, Zhong Q, 2021. In situ fabrication of cobalt/nickel sulfides nanohybrid based on various sulfur sources as highly efficient bifunctional electrocatalysts for overall water splitting. *Nano Select*, Vol. 3, pp. 147.

[14] Pintado S, Goberna-Ferrón S, Escudero-Adán EC, Galán-Mascarós JR, 2013. Fast and Persistent Electrocatalytic Water Oxidation by Co–Fe Prussian Blue Coordination Polymers. J. *Am. Chem. Soc.*, Vol. 135, pp. 13270–13273.

[15] Liang Z, Qu C, Zhou W, Zhao R, Zhang H, et al., 2019. Synergistic effect of Co-Ni hybrid phosphide nanocages for ultrahigh capacity fast energy storage. *Advance Science*, Vol. 6, pp. 1802005.

[16] Haber JA, Cai Y, Jung S, Xiang C, Mitrovic S, et al., 2014. Discovering Ce-rich oxygen evolution catalysts, from high throughput screening to water electrolysis. *Energy & Environmental Science*, Vol. 7, pp. 682-688.

[17] Wang X, Wang S, Chen S, He P, Xu Y, et al., 2020. Facile one-pot synthesis of binder-free nano/microstructured dendritic cobalt activated nickel sulfide: a highly efficient electrocatalyst for oxygen evolution reaction. *Int. J. Hydrog. Energy*, Vol. 45, pp. 19304.

[18] Wang Y, Yang C, Huang Y, Li Z, Liang Z, Cao G, 2020. Nickel induced electronic structural regulation of cobalt hydroxide for enhanced water oxidation. *J Mater Chem A*, Vol. 8, pp. 6699.

[19] Liang H, Meng F, Caban-Acevedo M, Li L, Forticaux A, et al., 2015. Hydrothermal continuous flow synthesis and exfoliation of NiCo layered double hydroxide nanosheets for enhanced oxygen evolution catalysis. *Nano Lett*., Vol. 15, pp. 1421.

[20] Suen NT, Hung SF, Quan Q, Zhang N, Xu YJ, Chen HM, 2017. Electrocatalysis for the oxygen evolution reaction: recent development and future perspectives. *Chem. Soc. Rev*., Vol. 46, pp. 337.